A simple method for detecting cracks in soil-cement reinforcement for centrifuge modelling

- Shuji Tamura, Dr. Eng

Associate Professor, Department of Architecture and Building Engineering,School of Environment and Society,Tokyo Institute of Technology, Tokyo, Japan

- Mohammad Khosravi, PhD

Postdoctoral Researcher, Department of Civil and Environmental Engineering, University of California, Davis, CA, USA

- Daniel Wilson, PhD

Associate Director, Center for Geotechnical Modeling, Department of Civil and Environmental Engineering, University of California, Davis CA, USA

- Deepak Rayamajhi, PhD

Geotechnical Engineer, CH2MHILL Inc., Corvallis, OR, USA

- Ross W. Boulanger, PhD

Professor, Department of Civil and Environmental Engineering, University of California, Davis CA, USA

- C. Guney Olgun, PhD

Research Assistant Professor, Via Department of Civil and Environmental Engineering, Virginia Tech, Blacksburg,VA, USA

- Yongzhi Wang, PhD

Associate Professor, Institute of Engineering Mechanics, China Earthquake Administration, Harbin, China

Full contact details of corresponding author.

Shuji TAMURA

Tokyo Institute of Technology

School of Environment and Society, Dept. of Architecture and Building Engineering

2-12-1-M1-33 Ookayama, Meguro-ku, Tokyo, 152-8550, JAPAN

E-mail: tamura@arch.titech.ac.jp

TEL: +81-3-5734-3161

Authors' copy submitted September 2017

Published with edits as Tamura, S., Khosravi, M., Wilson, D. W., Rayamajhi, D., Boulanger, R. W., Olgun, C. G., and Wang, Y. (2018). “A simple method for detecting cracks in soil-cement reinforcement for centrifuge modeling.” International Journal of Physical Modeling in Geotechnics, ahead of print, https://doi.org/10.1680/jphmg.17.00036.]

Abstract (150 words)

In this paper, we present the development, implementation, and experimental evaluation of a new crack detection mechanism for centrifuge modelling. The proposed mechanism is a brittle conductor bonded to cement providing a binary indication of if, and when, a sensor is cracked. The results of a pair of large centrifuge tests were used to evaluate the effectiveness of the proposed crack detection mechanism. Each test model included a soil profile consisting of a 23-m-thick layer of lightly over-consolidated clay, underlain and overlain by thin layers of dense sand. The centrifuge models had two separate zones, a zone without reinforcement and a zone with an "embedded" soil-cement grid which penetrated the lower dense sand layer and had a unit cell area replacement ratio A_r = 24%. Models were subjected to 13 different shaking events with peak base accelerations ranging from 0.005 to 0.55 g (prototype scale). The performance of the proposed crack detection mechanism was examined using 1) post-test crack mapping in the soil-cement grids, 2) results of the crack detection system, and 3) time series of accelerations, displacements, and footing rotation. Results from the centrifuge test showed that the proposed crack detection method accurately captured if, and when, cracking occurred in the soil-cement grid at the locations of the sensors.

Keywords

Centrifuge modelling; Ground improvement; Monitoring; Crack

List of notation (examples below)

CD is the crack detector

1. Introduction

Cracks are easily observed indications of damage in concrete structures. Cracking patterns and crack location, orientation, number, and distribution provide information about the performance of the structure and possible failure modes. Several studies have been performed, and different techniques have been developed to accurately estimate if and where cracking occurs in a concrete structure. These techniques are either based on measuring the change in response of the structure due to cracking, such as change in natural frequency (Adams et al. 1978, Ju et al. 1982, Salawu, 1997) and antiresonant frequency (Dilena and Morassi 2004), or using new technologies, such as image processing (Li et al. 1991, Sinha and Fieguth 2006), acoustic emission (AE) (Ouyang et al. 1991, Ohtsu 1996), and fiber-optic sensor (Gu et al. 2000, Habel and Krebber 2011), to directly measure the occurance of cracks. These methods for crack detection and characterization of concrete structures are limited for use in geotechnical centrifuge modelling by either high cost and complexity or inaccuracy during early stages of cracking.

Centrifuge modelling has been used extensively to investigate soil-cement reinforcement strategies (e.g., columns, walls, grids) for improving the performance of foundations for structures, embankments, slopes, earth retaining structures, tunnels, and seawalls. Soil-cement reinforcements are often used to remediate against ground deformations or failure modes in soft or liquefiable soils (e.g., Adalier et al. 1998, Kitazume and Maruyama 2006, Takahashi et al. 2006, Ishikawa and Asaka 2006). In most of these studies, acrylic or metal have been used to represent the soil-cement reinforcement within the centrifuge models. Few studies (e.g., Khosravi et al. 2016, Khosravi et al. 2017) have investigated the effect of partial damage and cracking of the structural reinforcing elements on the response of soil and structure system.

Currently applied methods for crack detection and characterization for above-ground concrete structures include periodic visual inspections, and non-destructive evaluation (NDE) such as a change in the frequency content of the system, or using AE and fiber-optic sensors. Visual inspection of cracking of underground structures (e.g., ground reinforcement) is practically impossible during the test. Post-test inspection of the cracks after excavation of the soil surrounding the structure provides useful information about the overall performance of the underground structure, but limited information can be obtained about possible failure modes and time of cracking. Change in the frequency content of the system is not a reliable technique to estimate cracking of underground structures since it can be affected by the response of surrounding soil and the interaction between the soil and underground structure. Using AE and fiber-optic sensors in geotechnical centrifuge is also difficult and expensive. An inexpensive alternative approach for estimating cracking in centrifuge testing is strain measurement. A large change in strain value is an indication of cracking in the structure. A strain gauge, however, measures strain at a local point and is also difficult to install on cast-in-place underground structures such as soil-cement ground reinforcement (e.g., grid or column). Chin et al. (2009) developed a simple and low-cost method for crack detection in concrete structures using a short,

narrow copper strip (GC Tool Pure Copper Circuit Tape 0.05 mm in thickness and 3.18 mm in width). In their method, the cracking of the concrete is characterized by a large and persistent voltage drop after breaking the copper strip. This type of concept has the potential for providing a more accurate, reliable, and affordable method for quasi-real-time crack detection and characterization for centrifuge modelling.

This paper describes a novel yet simple crack detection mechanism and its validation process in centrifuge testing to estimate the formation of cracks in soil-cement ground reinforcement. The proposed mechanism is a brittle conductor bonded to cement providing a binary indication of if, and when, cracking occurred. The crack detection system was used in a series of dynamic centrifuge tests, to investigate the performance of soil-cement grids during earthquake loading. The performance of the proposed crack detection system during shaking was investigated using (1) post-test crack mapping in the soil-cement grids, (2) results of the crack detection system, and (3) examination of time series of soil and footing response for evidence of consistency with the crack detection system.

2. Proposed crack detection technique in geotechnical centrifuge testing

A schematic of the crack detection mechanism used is shown in Fig. 1. The mechanism is a resistive voltage divider and includes two resistors, R_1 and R_2, connected in series, with the input voltage applied across the resistor pair and the output voltage emerging from the connection between them. The output voltage, V_{out}, is directly proportional to the input voltage, V_{in}, and the ratio of R_1 and R_2 and can be calculated using the following equation:

$$V_{out} = V_{in} \cdot \frac{R_2}{R_1 + R_2} \quad (1)$$

R_1 is a resister of 100k ohm, R_2 is the crack detector element. The idea was to select a brittle conductor that shows a large change in electric conductivity if an open crack develops anywhere along its length, similar to the concept used by Chin et al. (2009) for concrete structures. The change in electric conductivity is temporary if the crack later closes and contact is re-established between both sides of the cracked conductor.

Pencil lead made of graphite was used as the crack detector sensor in this study. Graphite is a semi-metal and an electrical conductor. The resistivity of a pure graphite is 0.0000138 ohm/meter. The resistance of graphite also varies with grades used in lead manufacturing. In this study, pencil leads with H, and 2H grades with resistance in the range of 20 to 25 ohm were used. Pencil lead can form a strong bond with the surrounding soil-cement material during curing. As shown in Fig. 2, wires are connected to each end of the pencil lead using heat-shrink tubing. The pencil lead crack sensor can be placed and sealed inside a groove in prefabricated columns and grids or can

be embedded in cast-in-place columns and grids before curing. The later approach was used herein.

3. Overview of centrifuge tests

The performance of the proposed crack detection mechanism was examined using dynamic centrifuge tests of a soft clay treated with a soil-cement grid. Centrifuge tests were performed using the 9.1-m radius centrifuge at the University of California at Davis, Center for Geotechnical Modelling using a "Hinged-Plate model Container (HPC)" under 57 g centrifugal acceleration. The detail of the centrifuge tests was described in the preliminary reports (Khosravi et al., 2015a, b).

The soil profile consisted of 410 mm thick (model scale) layer of slightly over-consolidated clay underlain by 40 mm thick saturated dense sand (Dr ≈ 90%) for drainage purpose. Test model had an unreinforced soil profile on the left end of the container and an embedded soil-cement grid at right end as shown in Fig. 3. The soil-cement grid was set on the base sand later. The clay layer was constructed by pre-consolidating the clay in six lifts using a hydraulic press. Soil-cement grid was constructed using the trench and excavation method as described in Khosravi et al. (2015b). In this method, first a mold consisting of nine 150 mm × 150 mm stainless steel square grids were fabricated. A wood frame was used to hold and align the steel grids while they were inserted into the consolidated clay (Fig. 4a). The spacing between the mold walls was equal to the required thickness for the soil-cement panels. The mold was pushed into the clay using a hydraulic press. The clay within the mold was excavated by hand using a spatula. Once sufficient excavation was complete, the mold walls were filled with soil-cement slurry (Fig. 4b). The steel plate grids were then pulled out and sensors were placed into the slurry at the target location (Fig. 4c). More details can be found in Khosravi et al. (2015b). The embedded grid, 530 mm (shaking direction) × 530 mm (width) × 410 mm (depth), had nine square cells in a three-by-three pattern. The 21 mm wide soil-cement walls were spaced 151 mm center-to-center apart, for an average area replacement ratio of A_r = 24%. Unconfined compressive strength of clay-cement mixture was 430 to 670 kPa after 7 days and 480 to 650 kPa after 14 days. A 40-mm-thick layer of coarse Monterey sand was placed over the clay surface as shown in Fig. 3. The soil-cement grid and the target unconfined compressive strength were designed based on references, Brown et al. (2013) and Bruce et al, (2010).

The 2-mm diameter pencil lead crack detectors (CDs) were embedded in the cast-in-place soil-cement grid before curing in order to form a strong bond with the surrounding soil-cement material during curing. Eighteen crack detectors, with lengths of 60 mm or 90 mm, were laid on the surface of the slurry grid either parallel or perpendicular to the direction of shaking and were then pressed into the slurry to a target depth. Locations and final depths are shown in Fig. 5. The numbers following sensor ID show the depth of crack detectors from the soil-cement mixture surface in model scale (mm). Models were also instrumented with accelerometers, pore water pressure transducers (PPTs), and linear potentiometers (LPs) as described in Khosravi et al. (2015a, b).

Test MKH01, before placement of the single degree of freedom (SDOF) structure on top of the grids, was shaken with 13 different motions with PBA ranging from 0.005 to 0.32 g as shown in Table 1 (prototype scale). Input motions were step motion, sine sweep motions (SW7-333), the 1999 Chi-Chi earthquake (TCU-078) and the 1995 Kobe earthquake (Kobe 0807). These shaking events were used to examine the effect of the soil-cement grids on dynamic site response. The dynamic responses of the reinforced soil profiles during those events and analyses of the soil-cement grids' reinforcing effects are described in Khosravi et al. (2016).

The SDOF structure was then placed over the central part of the grid system over the sand layer in Test MKH02 as shown in Fig. 3. The SDOF structure consisted of an aluminium square footing, a hollow rectangular aluminium column, and an aluminium and steel block superstructure. The mass of the superstructure, column, and footing were 4.8 kg, 0.2 kg, and 2.1 kg, respectively. The natural period of the structure was 71 Hz (model scale) under fixed base condition. The footing, with dimensions of 200 mm × 200 mm, covered the center grid element. The model, with the SDOF structures in place, was shaken with a sequence of 12 shaking events. The sequence of shaking events and their PVAs and PBAs are provided in Table 1.

4. Results and Discussion

Performance of crack detectors embedded in the soil-cement grid is examined using (1) post-test crack mapping in the soil-cement grids, (2) change in potential difference measurements (voltage output) of the crack detectors before, during, and after shaking, and (3) examination of time series of accelerations, displacements, and footing rotations for evidence of consistency with the crack detector measurements.

4.1 Post-test crack mapping in the soil-cement grids

After the completion of Test MKH01 (without structure), sand over the grid top was removed and cracking of the top of the grid was mapped from visual inspection. Fig. 5 shows a sketch of the locations of the observed cracks (blue lines) on the top of the soil-cement grid after the test. Cracking was very limited during the shaking events in Test MKH01, and a minor crack occurred near the location of CD04.

After the completion of Test MKH02 (with structure), all of the sand was carefully removed and cracking of the soil-cement grid was mapped during the model excavation. The locations of the observed cracks on the top of the soil-cement grid after the test were shown in Fig. 5 as red lines. Photographs of the embedded grid with the locations of the observed cracks are shown in Fig. 6. After test MKH02, the soil-cement walls showed extensive crushing and cracking beneath the structural footing, with crushing extending 5 to 9 mm below the tops of the walls and significant cracking to depths of up to 175 mm, as shown in Fig. 6. The cracking patterns evident in Figs. 5 and 6 demonstrate the significant effect of SDOF structure on the damage of the soil-cement grid

during shaking. Table 2 summarizes the conditions of the soil-cement grid at the location of the crack detectors after Test MKH02. Based on the visual inspection of the soil-cement grid after Test MKH02, cracking occurred through crack detectors CDs 03, 04, 06, 11, 12, 13, 14, 16, and 17.

4.2 Variation of voltage output during the centrifuge tests

Based on Eq. 1, for graphite with a resistance of approximately zero ohm, the electric potential difference between the two ends of the crack detector should be zero (or close to zero) before any crack develops along its length. An open “crack” (discontinuity) in the crack detector changes its conductivity and the electric potential difference between the two ends of the crack detector. The final voltage depends on the magnitude of the crack separations and/or offsets, as well as on the resistivity of the fluids or soil-cement fragments filling the cracks.

Fig. 7 summarizes the potential difference measurements (voltage outputs) between the two ends of the crack detectors during Test MKH01. Fig. 7 includes the measured voltage at the beginning of the tests, after the Kobe motion with PBA = 0.18 g, and at the end of the tests. Initial voltage outputs for all crack detectors were close to zero, as expected. During Test MKH01, change in voltage output of crack detector was only observed in CD04 during Kobe motion with PBA = 0.18 g. A hairline crack was observed near the location of CD04 in the post-test inspection of the soil-cement grid after Test MKH01 as shown in Fig. 5. The crack detector was at a depth of 40 mm (model-scale) from the top of the soil-cement grid. The results implied that the crack propagated through the depth, and crossed the crack detector. Changes in the voltage output of the other CDs were small. This was consistent with the post-test obeservation of the soil-cement grid during which no cracking was observed in CD’s locations except for CD04.

Dynamic responses (prototype) of the embedded grid in Test MKH01 are shown in Fig. 8 for Kobe motion with PBA = 0.18 g. This figure shows the input base motion, horizontal acceleration, relative displacement near the ground surface on the soil inside the grid cells and the mid points of the transverse walls (perpendicular to shaking), and the voltage output of crack detector CD04. The peak horizontal accelerations (PHA) on the soil surface and transverse wall were 0.43 g producing an amplification factor of 2.4 comparing to the base motion. As shown in Fig. 8c, the transverse wall experienced maximum relative displacement of about 23 mm comparing to the soil inside the grid cell at the time equal to 8 sec. This time corresponds to the onset of cracking in crack detector CD04 as presented in Fig. 8d. These results suggest that the soil inside and outside the grid imposed significant kinematic demands on the grid, causing cracking of the soil-cement. Crack detector CD04 showed that the crack closed during cyclic load reversals as the contact between both sides of the cracked conductor was re-established. Crack detector CD04 fully opened at about 14.0 sec and then closed after Test MKH01, when the model was returned to 1g.

The potential difference measurements (voltage outputs) between the two ends of crack detectors in the embedded grid in Test MKH02 are shown in Fig. 9, including voltages at the start of Test MKH02 (i.e., after the end of Test MKH01), after the strongest TCU motion with PBA = 0.32 g, after the strongest Kobe motion with PBA = 0.55 g, and at the end of Test MKH02 (i.e. when the model was returned to 1g). The voltage outputs increased at crack detectors CD06, CD11, CD12, and CD13 during TCU motion with PBA = 0.32 g. No new cracking developed during Kobe motion with PBA = 0.19 g. During Kobe motion with PBA = 0.54 g, the voltage outputs of four new crack detectors, CD03, CD14, CD16, and CD17 also increased. Post-test observation of the soil-cement grid showed cracks around these crack detectors as summarized in Fig. 5 and Table 2. In crack detectors with a small change in their voltage outputs, no cracking was observed at the CD locations during the post-test inspection of the grid. The results of this centrifuge test indicates that the proposed crack detection mechanism can accurately capture if, and when, cracking occurred in the soil-cement grid.

Dynamic responses (prototype) of the embedded grid and supported structure in Test MKH02 are shown in Fig. 10 for the strongest Kobe motion with PBA = 0.54 g. This figure presents the input base motion, horizontal acceleration and footing rotation. The voltage output of four crack detectors, CD03, CD14, CD16, and CD17, are also presented in Fig. 10. As shown in Figs. 10a and b, the surface acceleration had stronger long-period components than the base acceleration, which is attributed to softening of the soil and partial damage to the soil-cement grid, resulting in an effective lengthening of the reinforced soil system's effective natural period. We could not calculate the relative displacement between the panels and soil under the footing as the accelerometers over the soil-cement grid were removed before placing the SDOF system in Test MKH02 to prevent damaging of the sensors. Footing rotation was computed from the difference in vertical displacements across the footing width and is presented in Fig. 10c. As shown in Fig. 10c, the footing experienced four successive rotation cycles with a maximum value of 0.02 rad and accompanied by a permanent residual rotation of about 0.006 rad. As shown in Fig. 10d, in crack detectors CD14 and CD17 which were located on the northern side of the footing (Fig. 5) cracking started to develop at about 6.0 sec before footing started to rotate. In crack detectors CD03 and CD16, which were located on the southern side of the footing (Fig. 5), cracking occurred at about 8.0 sec which was also at the time of zero rotation. In Test MKH02, it is difficult to distinguish the cracking mechanism of the soil-cement grid. However, the results from crack detectors together with the measured response of soil and soil-cement grid can be used to better understand the complex interaction between soil, structure, and soil-cement grid.

4. Conclusions

The results from a pair of large centrifuge models were used to develop a new crack detection mechanism to measure the formation of cracks in a soil-cement ground reinforcement for centrifuge modelling. The mechanism includes a brittle conductor (pencil lead) providing a binary

indication of if, and when, a sensor is cracked. The centrifuge model tests included a soil profile reinforced with a soil-cement grid.

The performance of crack detectors embedded in the soil-cement grid was examined using change in potential difference measurements (voltage output) during shaking and after testing, and post-test crack mapping in the soil-cement grids. Results from centrifuge tests showed that the proposed crack detection mechanism accurately captured if, and when, the soil-cement grid cracked. Dynamic responses of soil, soil-cement grid, and structure together with results from crack detectors can be used to better understand the cracking mechanism of the soil-cement grid during different motions. Results indicated the importance of both loading from a superstructure and loading from soil in the performance of soil-cement grid.

Acknowledgements

This work was supported by the National Science Foundation (NSF) under Grant No. CMMI-1208117, Pacific Earthquake Engineering Research Center (PEER), Japan Society for the Promotion of Science (JSPS), Disaster Prevention Research Institute (DPRI), Kyoto University, and Key Laboratory of Earthquake and Engineering Vibration, Institute of Engineering Mechanics, CEA, China. Operation of the centrifuge facility was supported by NSF under Grant No. CMMI-0927178. Any opinions or conclusions expressed herein are those of the authors and do not necessarily reflect the views of NSF, PEER, JSPS, or DPRI. The authors appreciate the assistance of the staff of the Center for Geotechnical Modelling at the University of California at Davis. The authors would also like to thank Dr. Ivan Kraus, Faculty of Civil Engineering Osijek, University of Osijek, for a very helpful review and valuable comments and suggestions.

References

Adalier, K., Elgamal, A. K., and Martin, G. R. (1998). Foundation Liquefaction Countermeasures for Earth Embankments. J. of Geotech. and Geoenviron. Eng., 124(6), pp. 500-517.

Adams. R. D., Cawley, P., Pye, C. J. and Stone. B. J. (1978). A vibration technique for non-destructively assessing the integrity of structures, Journal of Mechanical Engineering Science, 20 (2), pp. 93-100.

Brown, D.A., Turner, J.P., and Castelli, R.J., (2010). "Drilled Shafts: Construction Procedures and LRFD Design Methods." Report No. FHWA NHI-10-016, Federal Highway Administration, Washington, DC.

Bruce, M.E.C., Berg, R.R., Collin, J.G., Filz, G.M., Terashi, M., and Yang D.S. (2013). "Deep Mixing for Embankment and Foundation Support." Report No. FHWA-HRT-13-046, Federal Highway Administration, Washington, DC.

Chin, J.-C., Rautenberg, J.M. Ma, C.Y.T., Pujol, S., Yau, D.K.Y. (2009). An Experimental Low-cost, Low-data-rate Rapid Structural Assessment Network. IEEE Sensors Journal, Special Issue on Sensor Systems for Structural Health Monitoring, 9(11), pp. 1361-1369.

Dilena, M., and Morassi, A. (2004). The use of antiresonances for crack detection in beams, Journal of Sound and Vibration, 276(1), pp. 195-214.

Gu, X., Chen, Z., and Ansari, F. (2000). Embedded fiber optic crack sensor for reinforced concrete structures. ACI Structural Journal, 97(3), pp. 468-476.

Habel, W.R. and Krebber, K., (2011). Fiber-optic sensor applications in civil and geotechnical engineering, Photonic Sensors, Volume 1(3), pp. 268-280.

Ishikawa, A., Asaka, Y., (2006). Seismic responses of column and grid-type improved grounds. hysical modelling in geotechnics, ICPMG '06 International conference 6th Physical modelling in geotechnics, ICPMG '06, pp.521-526.

Ju, F. D., Akgtin, M., Paez, T. L. and Wong, E. T. (1982). Modal method in diagnosis of fracture damage in simple structures, Productive Application of Mechanical Vibrations, Applied Mechanics Division. ASME, 52, pp. 113-126.

Khosravi, M., Wilson, D. W., Boulanger, R. W., Olgun, C. G., Tamura, S., and Wang, Y., (2015a). Test MKH01: Dynamic Centrifuge Tests of Soft Clay Reinforced by Soil-Cement Grids, Network for Earthquake Engineering Simulation (distributor), Dataset, doi:10.4231/D3HD7NT63

Khosravi, M., Wilson, D. W., Boulanger, R. W., Olgun, C. G., Tamura, S., and Wang, Y., (2015b). Test MKH02: Dynamic Centrifuge Tests of Structures on Soft Clay Reinforced by Soil-Cement Grids, Network for Earthquake Engineering Simulation (distributor), Dataset, doi:10.4231/D38P5VB1Q

Khosravi, M., Boulanger, R., Tamura, S., Wilson, D., Olgun, C., and Wang, Y. (2016). Dynamic Centrifuge Tests of Soft Clay Reinforced by Soil–Cement Grids. J. Geotech. Geoenviron. Eng., 10.1061/(ASCE)GT.1943-5606.0001487, 04016027.

Khosravi, M., Boulanger, R. W., Wilson, D. W., Olgun, C. G., Tamura, S., and Wang, Y. (2017). Dynamic centrifuge tests of structures with shallow foundations on soft clay reinforced by soil-cement grids, Soils and Foundations, Japanese Geotechnical Society, in-press.

Kitazume, M. and Maruyama, K. (2006). External stability of group column type deep mixing improved ground under embankment. Soils and Foundations, 16(3), pp. 323-340.

Li, L., Chan, P., and Lytton, R. L. (1991). Detection of thin cracks on noisy pavement images, Transportation Research Record, 1311, pp. 131-135..

Ohtsu, M. (1996). The history and development of acoustic emission in concrete engineering. Magazine of Concrete Research, 18(177), pp. 321-330.

Ouyang, C., Landis, E., and Shah, S. P. (1991). Damage assessment in concrete using quantitative acoustic emission. Journal of Engineering Mechanics, 117(11), pp. 2681-2698.

Salawu, O. S. (1997). Detection of structural damage through changes in frequency: a review. Engineering structures, 19(9), pp. 718-723.

Sinha, S. K., and Fieguth, P. W. (2006). Automated detection of cracks in buried concrete pipe images. Automation in Construction, 15(1), pp.58-72

Takahashi, H., Kitazume, M., Ishibashi, S. (2006). Effect of deep mixing wall spacing on liquefaction mitigation, Proc. of the 6th international conference on physical modelling in geotechnics, pp. 585-590.

Figure captions (images as individual files separate to your MS Word text file).

Figure 1. A schematic of the proposed crack detection mechanism

Figure 2. Details of the pencil lead crack detectors

Figure 3. Test MKH02 model configuration. Shaking direction was parallel to x-axis.

Figure 4. Soil-Cement Grid Construction Process: a) Grid Mold, b) Grid Mold inside the Clay, c) Soil-Cement Grid after Construction

Figure 5. Locations of cracks at the surface of the soil-cement grid after Test MKH01 (Blue Lines) and after Test MKH02 (Red lines). The numbers in brackets are the depth of crack detectors in mm (model scale) and the shadow area is the location of the footing.

Figure 6. Post-testing photographs of the embedded soil-cement grid in Test MKH02 with any visible cracks highlighted for clarity. Shaking was applied in the North-South (N-S) direction.

Figure 7. Voltage output of crack detectors at the beginning of Test MKH01, at the end of Kobe – PBA = 0.18g, and after Test MKH01.

Figure 8. Dynamic response of the embedded grid of Test MKH01 during Kobe motion with PBA = 0.18 g (prototype scale): (a) base acceleration; (b) soil and transverse wall acceleration; (c) transverse wall/soil relative displacement; (d) Voltage output of crack detector.

Figure 9. Voltage output of crack detectors at the beginning of Test MKH01, at the end of TCU (PBA = 0.32g), at the end of Kobe (PBA = 0.54g), and after Test MKH02.

Figure 10. Dynamic response of the embedded grid of Test MKH02 during the strongest Kobe motion with PBA = 0.54 g (prototype scale): (a) base acceleration; (b) soil and longitudinal wall acceleration; (c) Footing rotation; (d) and (e) Voltage output of crack detector.

Table 1. Ground motions at the base of the model container for Tests MKH01 and MKH02

Table 2. Conditions of soil-cement grid at the location of crack detectors after Test MKH02

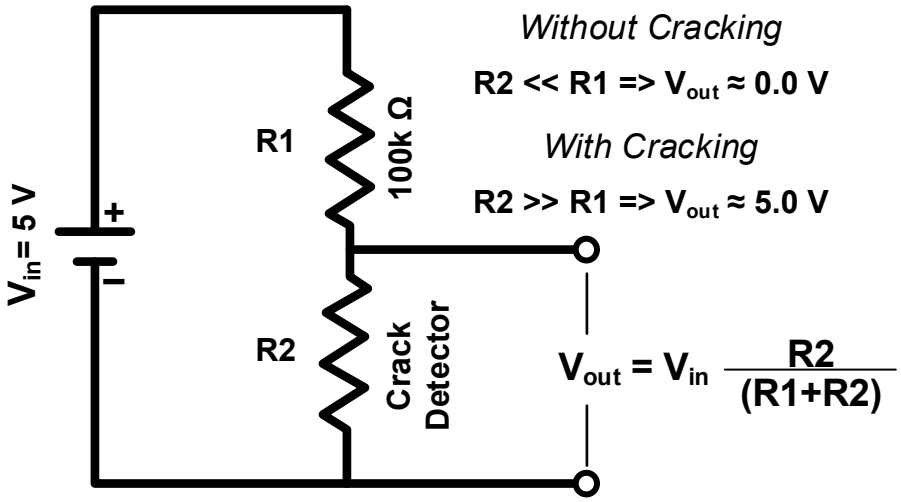

Figure 1. Simple resistive voltage divider

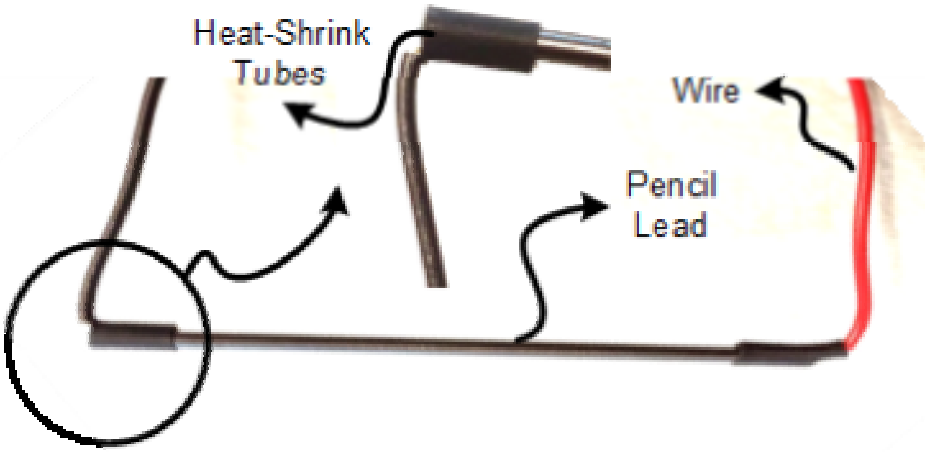

Figure 2. Details of the pencil lead crack detectors

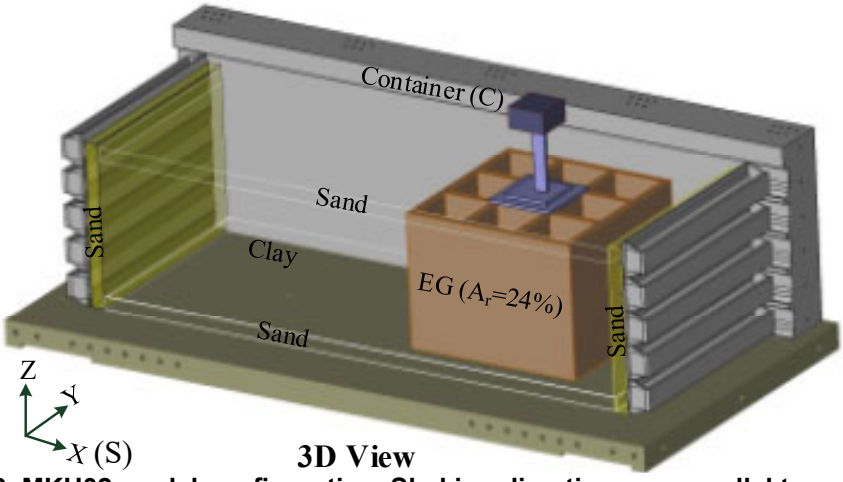

Figure 3. MKH02 model configuration. Shaking direction was parallel to x axis.

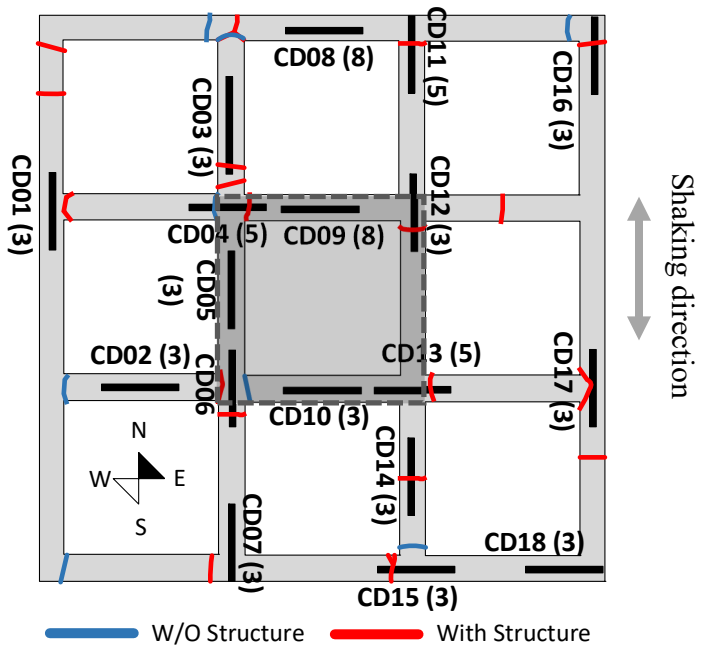

Figure 4. Locations of cracks at the surface of the soil-cement grid after Test MKH01 (Blue Lines) and after Test MKH02 (Red lines). The numbers in brackets are the depth of crack detectors in cm (model scale) and the shadow area is the location of the footing.

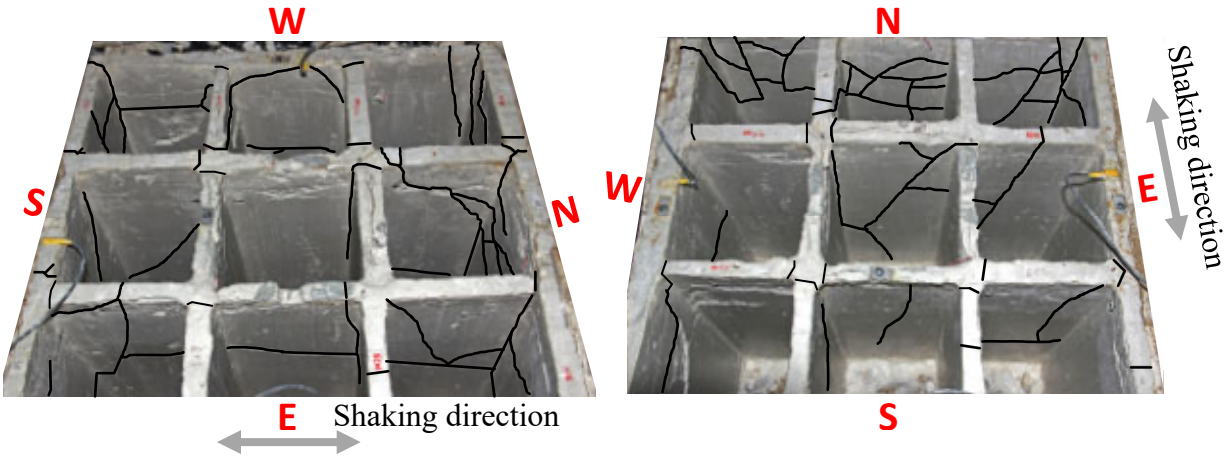

Figure 5. Post-testing photographs of the embedded soil-cement grid in MKH02 with any visible cracks highlighted for clarity. Shaking was applied in the North-South (N-S) direction.

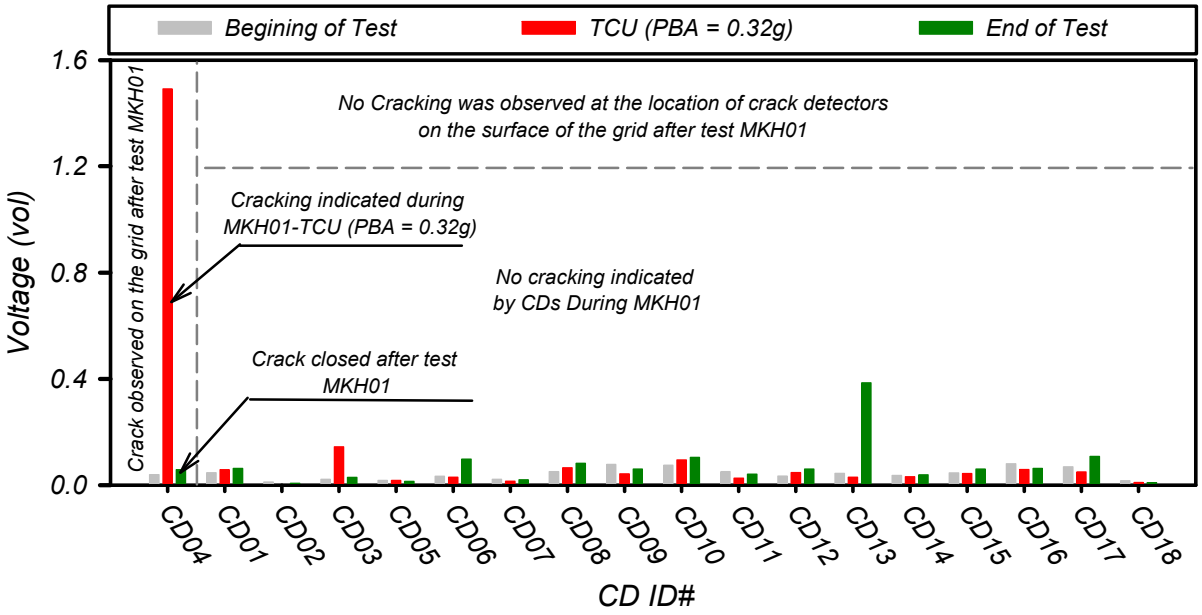

Figure 6. Voltage Output of Crack Detectors at the beginning of test, at the end of TCU – PBA = 0.32g, and after test in Test MKH01.

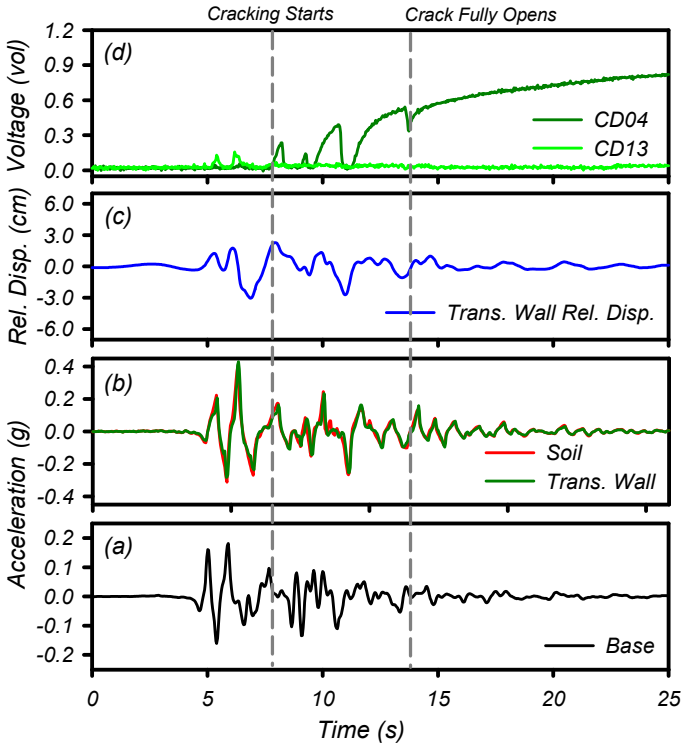

Figure 7. Dynamic response of the embedded grid (EG with A_r = 24%) of MKH01 during Kobe motion with PBA = 0.19 g (prototype scale): (a) base acceleration time history; (b) soil and transverse wall acceleration time histories (c) transverse wall/soil relative displacement time history; (d) Voltage output of crack detector time history.

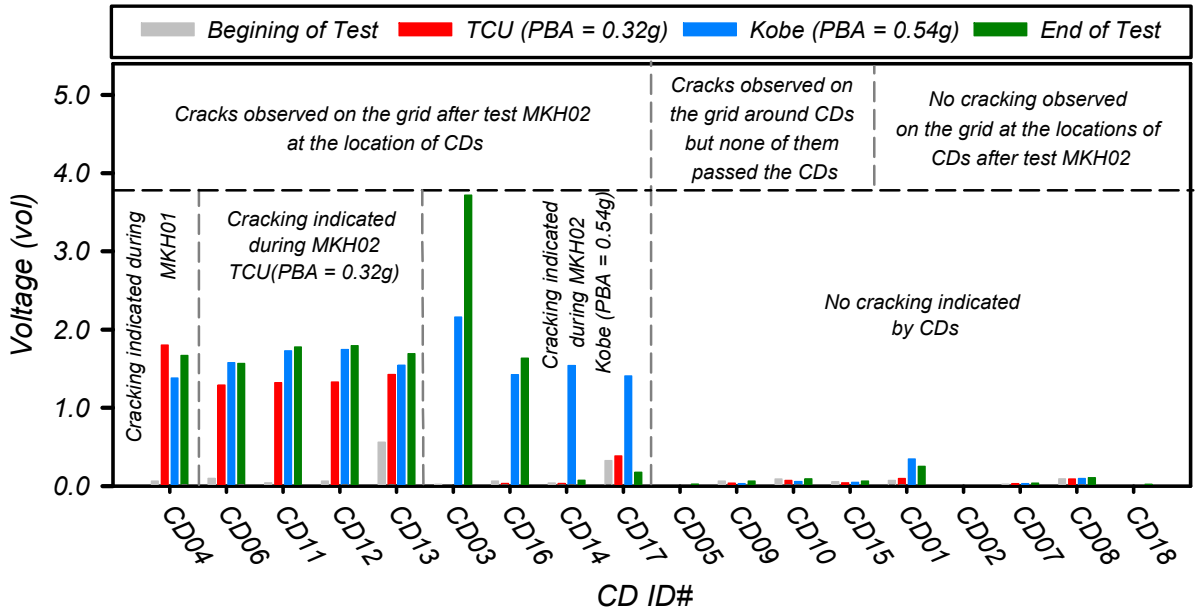

Figure 8. Voltage Output of Crack Detectors at the beginning of test, at the end of TCU (PBA = 0.32g), at the end of Kobe (PBA = 0.54g), and after test in Test MKH02.

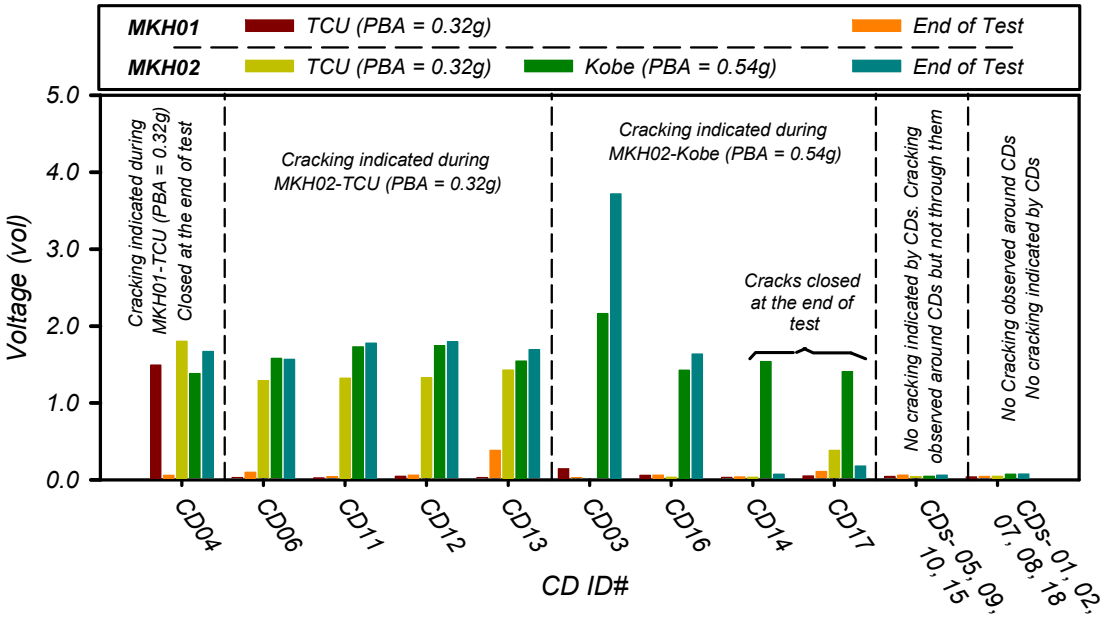

Figure 9. Voltage Output of Crack Detectors After All Shakings in test MKH01, at the end of test MKH01, at the end of TCU (PBA = 0.32g) in test MKH02, at the end of Kobe (PBA = 0.54g) in Test MKH02, after Spinning down in Test MKH02.

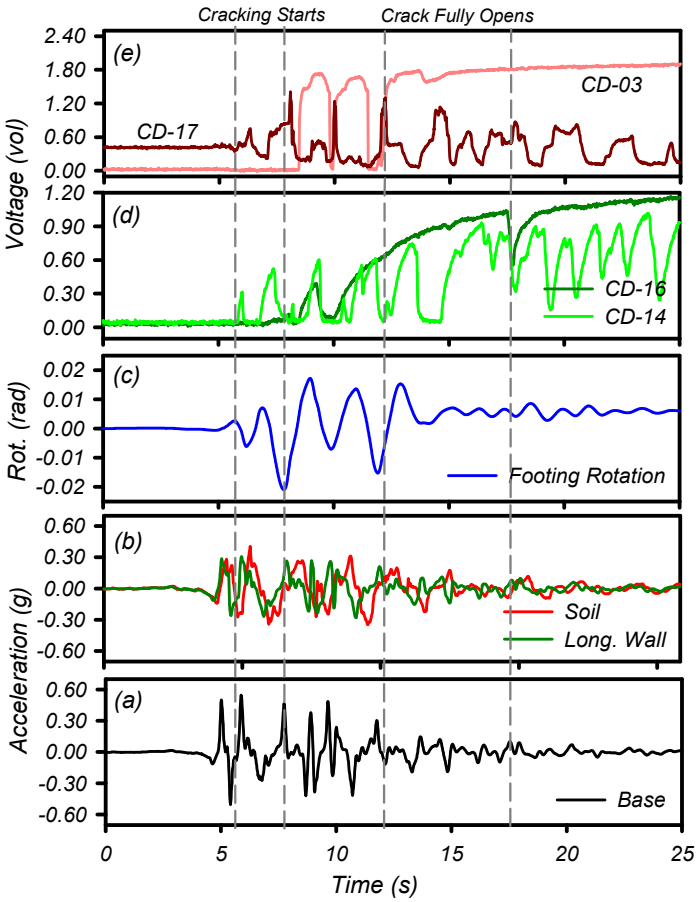

Figure 10. Dynamic response of the embedded grid (EG with A_r = 24%) of MKH02 during the strongest Kobe motion with PBA = 0.54 g (prototype scale): (a) base acceleration time history; (b) soil and longitudinal wall acceleration time histories; (c) Footing rotation time history; (d) and (e) Voltage output of crack detector time history.

Table 1. Ground motions at the base of the model containers for models MKH01 and MKH02

Event No.	Motion Name	MKH01 PBA g	MKH01 PBV cm/s	Event No.	Motion Name	MKH02 PBA g	MKH02 PBV cm/s
1	Step	0.005	0.86	1	Step	0.006	0.81
2	SW7-333	0.025	4.32	2	SW7-333	0.03	3.77
3	TCU 078	0.074	6.5	3	TCU 078	0.083	7.5
4	Kobe 0807	0.042	6.64	4	Kobe 0807	0.042	6.67
5	SW7-333	0.025	3.49	5	SW7-333	0.031	3.71
6	TCU 078	0.174	15.02	6	TCU 078	0.178	15.57
7	Kobe 0807	0.09	12.35	7	Kobe 0807	0.089	12.79
8	SW7-333	0.029	3.65	8	SW7-333	0.031	3.58
9	TCU 078	0.316	25.3	9	TCU 078	0.323	26.18
10	Kobe 0807	0.181	24.33	10	Kobe 0807	0.188	23.86
11	SW7-333	0.03	5.15	11	SW7-333	0.033	4.09
12	SW7-333	0.03	3.59	12	Kobe 0807	0.546	58.58
13	SW7-333	0.031	3.76	13	SW7-333	-	-

Table 2. Conditions of soil-cement grid at the location of crack detectors after test MKH02

CD No.	Condition near crack detectors
CD01	No Crack
CD02	No Crack
CD07	No Crack
CD08	No Crack
CD18	No Crack
CD03	Cracks all around CD
CD05	Horizontal cracks, no cracking pass through CD
CD10	Cracks parallel to CD, but no cracking pass through CD
CD09	Cracks parallel to CD, but no cracking pass through CD
CD17	Hair cracks around CD, no cracking pass through CD
CD15	Vertical crack stop at CD
CD04	Cracked
CD06	Cracked
CD11	Big crack was observed cutting crack detector
CD12	Vertical crack pass through CD
CD13	Vertical crack pass through CD
CD14	Hairline crack
CD16	Vertical cracks is wide open on the surface, but not major in lower depth

Table 3. A summary of centrifuge test chronology

Test	Event	PGA (g)	Sensor Condition
MKH01	Start Spinning	-	No Cracking
	SineSweep Motion	≈ 0.03	No Cracking
	TCU Motions	≤ 0.32	No Cracking
	Kobe Motions	≤ 0.09	No Cracking
	Kobe Motion	≈ 0.18	CD04 Cracked
	Spinning Down	-	CD04 Closed
MKH02	Start Spinning	-	CD04 Opened
	SineSweep Motions	≈ 0.03	No New Cracking
	TCU Motions	≤ 0.32	No New Cracking
	TCU Motion	≈ 0.32	CDs - 06,11,12,13 Cracked
	Kobe Motions	≤ 0.18	No New Cracking
	Kobe Motion	≈ 0.54	CDs - 03,14,16, 17 Cracked
	Spinning Down	-	CDs-14, 17 Closed